# Supplemental Material for
# Fabry-Pérot interference in gapped bilayer graphene with broken anti-Klein tunneling

Anastasia Varlet,[1,*] Ming-Hao Liu (劉明豪),[2] Viktor Krueckl,[2] Dominik Bischoff,[1] Pauline Simonet,[1] Kenji Watanabe,[3] Takashi Taniguchi,[3] Klaus Richter,[2] Klaus Ensslin,[1] and Thomas Ihn[1]

[1]*Solid State Physics Laboratory, ETH Zürich, 8093 Zürich, Switzerland*
[2]*Institut für Theoretische Physik, Universität Regensburg, D-93040 Regensburg, Germany*
[3]*Advanced Materials Laboratory, National Institute for Materials Science, 1-1 Namiki, Tsukuba 305-0044, Japan*

(Dated: June 13, 2014)

## I. THEORY

### A. Electrostatic model for the device

We apply the parallel-plate capacitor model to deduce the top- and back-gate efficiencies for our bilayer graphene (BLG) device. The thicknesses of the top and bottom hexagonal boron nitride (h-BN) layers are $d_{\text{h-BN}}^{(\text{top})} = 30\,\text{nm}$ and $d_{\text{h-BN}}^{(\text{bot})} = 23\,\text{nm}$, respectively, and we adopt $\varepsilon_r^{\text{h-BN}} = 3.0$ as their dielectric constant. The topgate capacitance for area C is then given by

$$\frac{C_{\text{TG}}}{e} = \frac{\varepsilon_r^{\text{h-BN}}\varepsilon_0}{e d_{\text{h-BN}}^{(\text{top})}} = 5.53\times10^{11}\,\text{cm}^{-2}\,\text{V}^{-1}. \tag{S1}$$

Together with the $SiO_2$ substrate with thickness $d_{SiO_2} = 285\,\text{nm}$ and dielectric constant $\varepsilon_r^{SiO_2} = 3.9$, the backgate capacitance is given by

$$\frac{C_{\text{BG}}}{e} = \frac{\varepsilon_0}{e}\left(\frac{d_{\text{h-BN}}^{(\text{bot})}}{\varepsilon_r^{\text{h-BN}}} + \frac{d_{SiO_2}}{\varepsilon_r^{SiO_2}}\right)^{-1} = 6.53\times10^{10}\,\text{cm}^{-2}\,\text{V}^{-1}. \tag{S2}$$

Next, we deduce the intrinsic doping by inspecting the full conductance map. We assume that in region $X$ ($X = \text{L},\text{C},\text{R}$), the residual carrier density is uniformly described by $n_X^0$. In Fig. 1(d) of the main text, the conductance dip at $V_{\text{TG}} = -2.1\,\text{V}$ along the $V_{\text{BG}} = 0\,\text{V}$ horizontal line cut suggests

$$n_{\text{C}}^0 = \frac{C_{\text{TG}}}{e}\times 2.1\,\text{V} = 1.16\times10^{12}\,\text{cm}^{-2}. \tag{S3}$$

For the outer areas L and R, the residual density is deduced from the two topgate-independent horizontal Dirac lines, one at $V_{\text{BG}} = -7.6\,\text{V}$, suggesting

$$n_{\text{L}}^0 = \frac{C_{\text{BG}}}{e}\times 7.6\,\text{V} = 4.97\times10^{11}\,\text{cm}^{-2}, \tag{S4}$$

and one at $V_{\text{BG}} = -14\,\text{V}$, suggesting

$$n_{\text{R}}^0 = \frac{C_{\text{BG}}}{e}\times 14\,\text{V} = 9.15\times10^{11}\,\text{cm}^{-2}. \tag{S5}$$

Collecting Eqs. (S1)–(S5), we obtain the gate-dependent carrier density:

$$n_X(V_{\text{TG}},V_{\text{BG}}) = \begin{cases} \dfrac{C_{\text{TG}}}{e}V_{\text{TG}} + \dfrac{C_{\text{BG}}}{e}V_{\text{BG}} + n_X^0, & X = \text{C} \\ \dfrac{C_{\text{BG}}}{e}V_{\text{BG}} + n_X^0, & X = \text{L},\text{R} \end{cases}. \tag{S6}$$

### B. Asymmetry parameter

To calculate the gate-dependent asymmetry parameter for our device, we follow the review by McCann and Koshino [1]. Let us temporarily suppress the area index $X$ and consider the total carrier density $n = n_t + n_b + n_0$, where $n_t$ is the topgate contribution, $n_b$ is the backgate contribution, and the intrinsic doping is assumed to be equally distributed in the two graphene layers: $n_{b0} = n_{t0} = n_0/2$. This assumption allows us to rewrite Eq. (65) of Ref. 1 as

$$U_{\text{ext}} = \frac{\gamma_1}{n_\perp}\Lambda(n_b - n_t), \tag{S7}$$

where

$$\Lambda = \frac{c_0 e^2 n_\perp}{2\gamma_1\varepsilon_r\varepsilon_0} \tag{S8}$$

is the screening parameter, and

$$n_\perp = \frac{\gamma_1^2}{\pi\hbar^2 v_F^2} \tag{S9}$$

is the characteristic carrier density. In Eqs. (S7)–(S9), $\gamma_1 = 0.39\,\text{eV}$ is the nearest-neighbor hopping for the interlayer coupling, $c_0 \approx 0.335\,\text{nm}$ is the interlayer spacing of the BLG, $\varepsilon_r = 1$ is the effective dielectric constant between the two layers of BLG, and $v_F$ is the Fermi velocity of graphene related to the tight-binding parameters through $\hbar v_F = (3/2)ta$, $t \approx 3\,\text{eV}$ being the nearest-neighbor intralayer hopping and $a \approx 0.142\,\text{nm}$ being the carbon-carbon bond length. Using Eq. (S7), Eq. (74) of Ref. 1 reads

$$\frac{n_\perp u}{\Lambda(n_b - n_t)} \approx \left[1 - \frac{\Lambda}{2}\ln\left(\frac{|n|}{2n_\perp} + \frac{1}{2}\sqrt{\left(\frac{n}{n_\perp}\right)^2 + \left(\frac{u}{2}\right)^2}\right)\right]^{-1}, \tag{S10}$$

* varleta@phys.ethz.ch

where $u = U/\gamma_1$ is defined. Finally, we rewrite Eq. (S10) as

$$u = \frac{\Lambda(n_b - n_t)}{n_\perp}\left[1 - \frac{\Lambda}{2}\ln\left(\frac{|n|}{2n_\perp} + \frac{1}{2}\sqrt{\left(\frac{n}{n_\perp}\right)^2 + \left(\frac{u}{2}\right)^2}\right)\right]^{-1} \tag{S11}$$

in order to avoid the divergence at $n_b = n_t$.

The nonlinear Eq. (S11) can be solved numerically to obtain the asymmetry parameter $U = \gamma_1 u$, when the inputs $n_t$, $n_b$, and $n_0$ are given. Using Eqs. (S3)–(S6) we obtain the asymmetry parameters $U_X$ for the respective areas $X = \mathrm{L}, \mathrm{C}, \mathrm{R}$ of our BLG device. Numerical results are shown in Fig. S1. The actual size of the band gap $U_g$ is related with $U$ through $U_g = |U|\gamma_1/\sqrt{\gamma_1^2 + U^2}$.

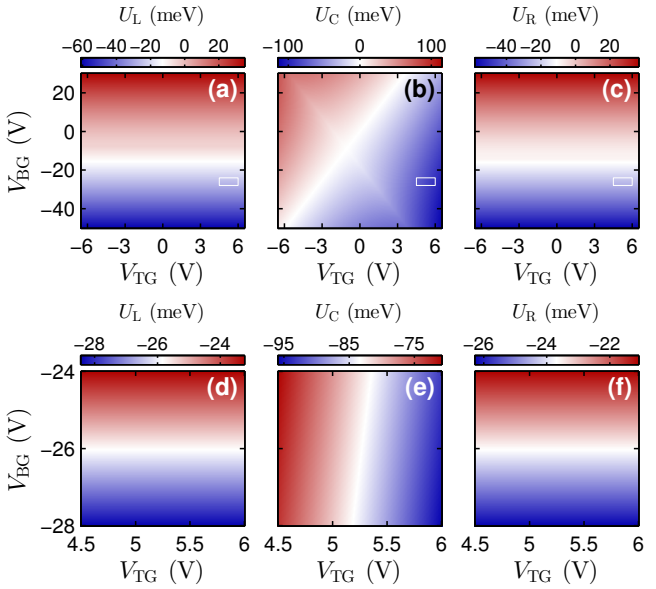


FIG. S1. Asymmetry parameter $U_X$ in region $X = \mathrm{L}, \mathrm{C}, \mathrm{R}$ of the device as a function top- and back-gate voltages. Panels (a)–(c) in the upper row show the full range, where the white boxes mark zoom-in range for panels (d)–(f) in the lower row.

### C. Local energy band offset

From the calculated carrier density $n_X$ and asymmetry parameter $U_X$ based on the electrostatic model, the band offset $V_X$ for area $X$ is given by

$$V_X = -\,\mathrm{sgn}(n_X)\sqrt{\frac{\gamma_1^2}{2} + \frac{U_X^2}{4} + \hbar^2 v_F^2 \pi |n_X| - \frac{\gamma_1}{2}\sqrt{\gamma_1^2 + (2\hbar v_F)^2 \pi |n_X|\left(1 + \frac{U_X^2}{\gamma_1^2}\right)}}, \tag{S12}$$

which is obtained by replacing the two-dimensional wave vector $k$ by $\sqrt{\pi|n_X|}$ in the energy dispersion $E(k)$ for gapped BLG [1] and by adding the minus sign. Application of Eq. (S12) on the diagonal matrix elements of the model Hamiltonian for transport calculation therefore fixes the global Fermi level at energy $E = 0$, at which the transmission function is evaluated (linear-response transport).

### D. Berry phase in gapped bilayer graphene

In order to take into account the characteristic band structure of the BLG, we incorporate the Berry phase into the resonance condition of the Fabry-Pérot (FP) oscillations in Eq. (1) of the main text. Therefore, we describe the low energy excitations of BLG for a single valley by the Hamiltonian [1],

$$H = \begin{pmatrix} U/2 & \hbar v_F k_- & 0 & 0 \\ \hbar v_F k_+ & U/2 & \gamma_1 & 0 \\ 0 & \gamma_1 & -U/2 & \hbar v_F k_- \\ 0 & 0 & \hbar v_F k_+ & -U/2 \end{pmatrix}, \tag{S13}$$

using the layer coupling $\gamma_1$, the asymmetry $U$ and $k_\pm = k_x \pm \mathrm{i}k_y$. Without losing generality we focus on a single valley, as the results of the second one can be obtained by time reversal, leading to an inverted Berry phase. The four eigenstates $\psi_\sigma(\boldsymbol{k})$ of $H$ can be associated with the different bands, which we label as $\sigma = n2, n1, p1, p2$ from high to low energy. [For the present discussion, the relevant bands are the two inner bands $n1, p1$ as those sketched in Fig. 1(f) of the main text.] Using these eigenstates, we can calculate the Berry curvature [2],

$$\mathscr{A}_\sigma(\boldsymbol{k}) = -\mathrm{i}\langle\psi_\sigma(\boldsymbol{k})|\nabla_k\psi_\sigma(\boldsymbol{k})\rangle\,, \tag{S14}$$

and the corresponding Berry phase

$$\Phi_\sigma = \oint_{k=\mathrm{const}} \mathscr{A}_\sigma(\boldsymbol{k})\cdot\mathrm{d}\boldsymbol{k}\,, \tag{S15}$$

which describes the additional phase the state $\psi_\sigma(\boldsymbol{k})$ picks up upon traveling adiabatically one complete circle in momentum space. Since transport within the central area C in the pn'p regime is carried only by the $n1$ band as sketched in Fig. 1(f) of the main text, FP oscillations pick up the Berry phase $\Phi_\mathrm{Berry} = \Phi_{\sigma=n1}$. This additional phase changes upon varying the top- and back-gate voltages in the whole possible range from 0 to $2\pi$, as shown in Fig. S2(a). Also for the experimental transport data presented in Fig. 2(a) of the main text, the Berry phase $\Phi_\mathrm{Berry}$ is not constant but takes values

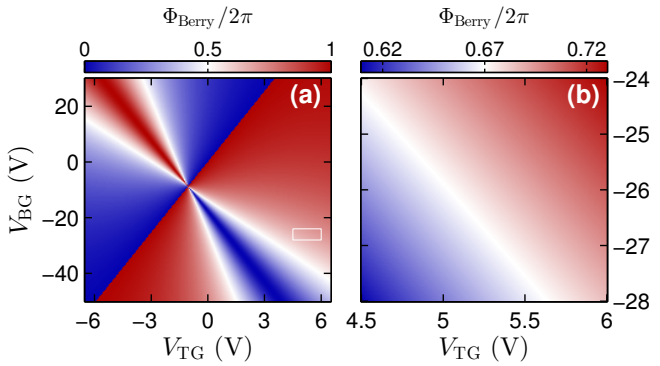


FIG. S2. (a) Berry phase as a function of top- and back-gate voltages for the state closest to the avoided crossing at the Dirac point within the dual-gated area C of the device. (b) Zoom-in of the bipolar block indicated by the white box in (a).

between $1.22\pi$ and $1.46\pi$, as presented in Fig. S2(b). Consequently, the Berry phase has to be included in the resonance condition in order to achieve a precise prediction of the conductance maxima.

## II. EXPERIMENT

### A. Oscillations: conductance VS transconductance signals

In the manuscript, we characterized the FP oscillations by studying the measured transconductance signal. The reason is a better visibility in the signal. However, the oscillations are already visible in conductance, as shown in Fig. S3(a-c). Their visibility is only weakened by the ascending slope (see Fig. S3(c)). The same analysis as the one done in the main manuscript could be performed with the conductance data.

### B. Density dependence

As explained in [3], Fabry-Pérot interference should give rise to oscillations spaced in density by $\Delta n = 2\sqrt{\pi n_C}/L_C$, where $n_C$ is the density in dual-gated area and $L_C$ the width of the cavity. In this case, $L_C = 1.1\ \mu$m. To confirm the origin of the oscillatory signal, we therefore study the peak spacing dependence, as done in the main text with Fig. 2(c), but on a broader range of voltages. To highlight the square root dependence, we show in Fig. S4(a) more data points: each color corresponds to a different backgate voltage value. We see that the observed behavior follows the expected behavior, represented with the black dashed line, reasonably well.

### C. Temperature dependence of the Fabry-Pérot oscillations

We observed in Fig. 4(c) of the main text that, at high temperatures, the oscillation amplitude saturates. This means that

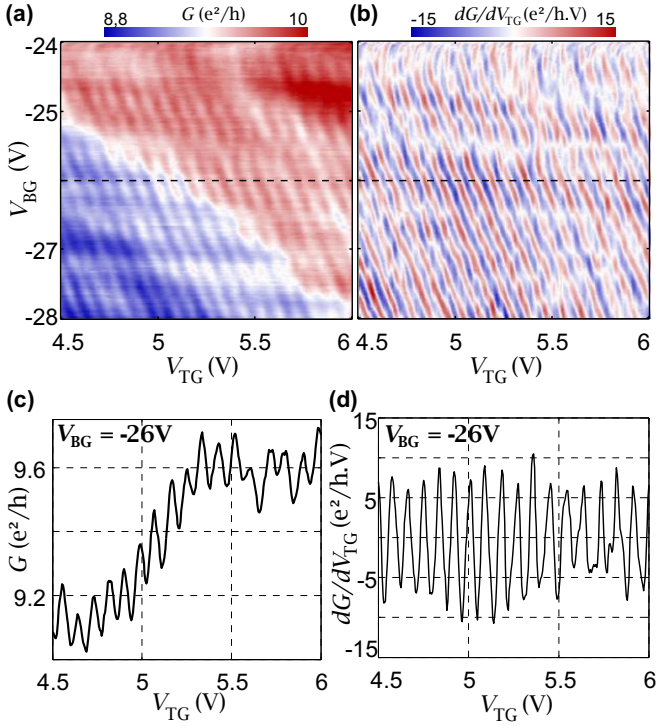


FIG. S3. (color online). (a) Conductance map corresponding to the measurement shown in Fig. 2(a) of the main text: the oscillations are already visible. (b) Normalized transconductance map (same as Fig. 2(a) of the main text, for comparison): the oscillations appear more clearly. (c)/(d) Cut taken from (a)/(b) at $V_{BG} = -26$ V.

part of the oscillations have a non-coherent origin and for further analysis, we subtract the highest temperature curve from each temperature signal.

To get a better insight in the observed temperature dependence, we consider the derivative of the Fermi-Dirac distribution:

$$\frac{\partial f}{\partial E_F} = \frac{1}{4k_BT}\frac{1}{\cosh^2\left(\frac{E-E_F}{2k_BT}\right)}, \tag{S16}$$

where $T$ is the fixed temperature (estimated from the recorded Allen-Bradley resistance value) and $E = \hbar^2\pi n_C/2m^*$.

Convoluting each measured trace with the derivative of the Fermi-Dirac distribution at $T = T_{\text{measured}}$, we notice that we do not recover the full amplitude of the measured signal. This can be due to a wrong evaluation of the energy (maybe due to screening or deformation of the band structure by trigonal warping, which are not taken into account here). To correct this parameter, we fit the convoluted curve using the temperature as a free parameter. The result is shown in Fig. S5(a).

Using these corrected temperatures, we now compare the standard deviation of each curve with the thermal damping term:

$$\frac{dG}{dV_{TG}} \sim A\frac{2\pi^2k_bT}{\Delta E}\frac{1}{\sinh\left(\frac{2\pi^2k_bT}{\Delta E}\right)}, \tag{S17}$$

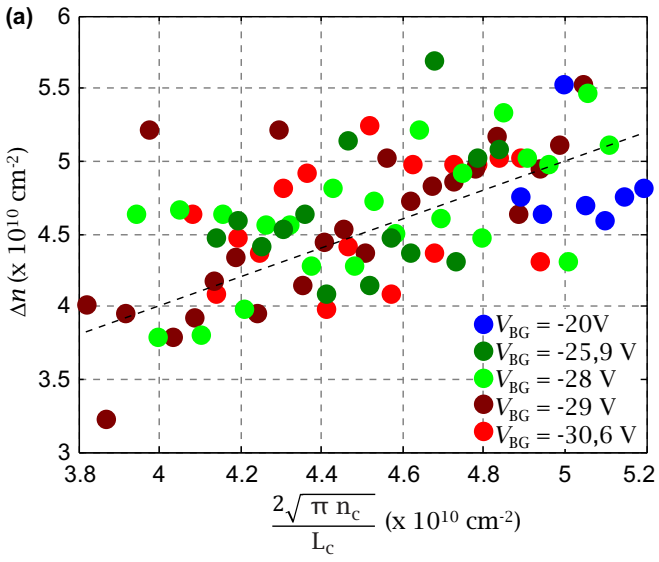


FIG. S4. (color online). (a) Dependence of the peak spacing as a function of density for different backgate voltages (different colors). The expected behavior is displayed in black dashed line.

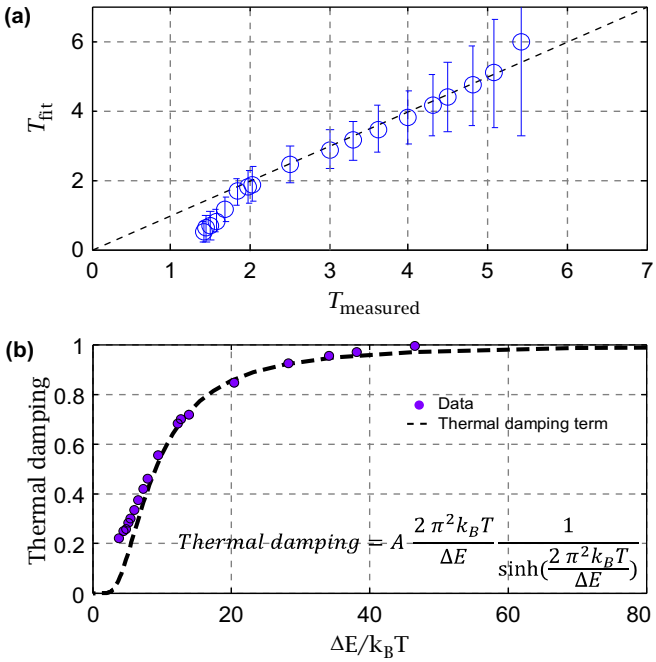


FIG. S5. (color online). (a) Result of the temperature fit compared to the measured temperature. (b) Using the fitted temperature value, we compare the behavior of our signal with the thermal damping (black dashed line).

with $A$ a scaling parameter and $\Delta E$ is the averaged period of the oscillations on the studied interval. The result is displayed in Fig. S5(b), with $A = 0.2$ and $\Delta E = 1.2$ meV. We find good agreement between the data points and the model and therefore attribute the damping of the oscillations as a function of temperature to thermal averaging.

[1] E. McCann and M. Koshino, Rep. on Progr. in Phys. **76**, 056503 (2013).
[2] M. V. Berry, Proc. R. Soc. Lond. A **392**, 45 (1984).
[3] A. L. Grushina, D.-K. Ki, and A. F. Morpurgo, Appl. Phys. Lett. **102**, 223102 (2013).